Asian Journal of Chemistry; Vol. 30, No. 3 (2018), 491-498

ASIAN JOURNAL OF CHEMISTRY

https://doi.org/10.14233/ajchem.2018.20895

Immobilization of Bi_2O_3 Particles on Activated Carbon Fiber and Its Photodegradation Performance for Pollutant Dyes

DINH CUNG TIEN NGUYEN, DONG-HYEN OH and WON-CHUN OH*

Department of Advanced Materials Science & Engineering, Hanseo University, Seosan-si, Chungnam 356-706, Republic of Korea

*Corresponding author: Tel: +82 41 6601337, E-mail: wc_oh@hanseo.ac.kr

Received: 30 June 2017; *Accepted*: 29 September 2017; *Published online*: 31 January 2018; AJC-18730

A combination of activated carbon fiber and bismuth oxide (Bi_2O_3) was prepared using a facile, one-step hydrothermal method. The resulting photocatalysts were characterized using X-ray diffraction, scanning electron microscopy, energy dispersive X-ray analysis, FT-IR spectra and BET method. UV-spectrophotometry was employed to measure the decrease in the concentration of rhodamine B, methylene blue trihydrate and reactive black B dyes in an aqueous solution after degradation with the photocatalysts under irradiation with visible light. The results contributes a new material to photocatalytic activity.

Keywords: Activated carbon fibers, Bismuth oxide, Photodegradation, Composite, Organic dyes.

INTRODUCTION

Bismuth oxide (Bi_2O_3) offers many outstanding properties and has been extensively used in many different fields such as catalysis [1,2], energy materials [3,4], optoelectronics, optical coatings [5], *etc*. due to its high refractive index, large energy band gap (2-3.96 eV) and dielectric permittivity [6]. The material with bismuth ingredient has been found to be a potential candidate for catalysis that can degrade organic pollutants under UV-visible light [7-9]. Besides, the preparation of bismuth particles with different routes by using a chemical method such as pyrolysis of bismuth compound [10,11], hydrochemical method [12-15] and solid state reaction [16] also attracted much attention of scientists. Mallahi *et al*. [17] reported about the synthesis and characterization of bismuth oxide nanoparticles *via* sol-gel method. Oudghiri-Hassani *et al*. [6] reported the synthesis, characterization and photocatalytic activity of α-Bi_2O_3 nano-particles.

On the other aspect, activated carbon fiber (ACF) is known as substrate source for synthetic nanomaterials that have many different targets, using a variety of synthetic approaches and combined with many types of nanomaterials. This material source is identified as the good candidate for preparing nanocomposite materials due to its high porosity and surface adsorption reactivity (1000 m^2/g) as well as larger pore volume than granular activated carbon (GAC) [18-22]. With several outstanding properties and functional groups on its surface, activated carbon fiber (ACF) is promising to make a positive effect in the photocatalyst activity [23]. One of the highlights of this material source is no significant effect on its adsorptive capacity with the change of pH value and temperature [24]. Yao *et al*. [25] reported the immobilization of TiO_2 nanoparticles on activated carbon fiber and its photodegradation performance for organic pollutants. Li *et al*. [26] reported the synergetic effect between adsorption and photodegradation on nanostructured TiO_2/activated carbon fiber felt porous composites for toluene removal. Nevertheless, the synthesis of ACF-Bi_2O_3 composite using a facile method, such as the hydrothermal method, however, the subsequent use of the materials have not been demonstrated yet.

To this end, a combination of activated carbon fiber (ACF) and Bi_2O_3 was prepared using a facile, one-step hydrothermal method and were used in the photodegradation of model organic pollutants rhodamine B, methylene blue trihydrate and reactive black B in an aqueous solution under visible light irradiation. The obtained solution was then transferred into an autoclave for the hydrothermal reaction. The structure and morphology of $Bi(NO_3)_3{\cdot}5H_2O$-ACF composites were characterized *via* X-ray diffraction (XRD), scanning electron microscopy (SEM), energy dispersive X-ray (EDX) analysis and FT-IR spectra. The surface area of the surveys composites were determined by using the BET method.

EXPERIMENTAL

Activated carbon fiber (ACF) was obtained from Nantong Sutong Carbon Fiber Co. Ltd. (Jiangsu, China). Bismuth nitrate pentahydrate (98 %), rhodamine B and methylene blue trihydrate were purchased from Samchun Pure Chemicals Co. Ltd., Korea. Reactive black B was purchased from JAY Chemical Industries

Ltd., India. Hydrochloric acid (35-37 %) and ethanol (95 %) were purchased from Duskan Pure Chemicals Co. Ltd., Korea. Sulfuric acid (98 %) was purchased from Daejung, Korea. All the chemicals were used without further purification and the double distilled water was used throughout the experiments.

X-ray diffraction (Shimadzu XD-D1) was used to determine the crystallinity with monochromatic high-intensity CuK_α radiation ($\lambda = 1.5406$ Å). Scanning electron microscopy (JSM-5600) was used to observe the surface and structure of the prepared composites. Elemental mapping over the desired region of prepared composite was detected using an energy dispersive X-ray (EDX) analysis attached to SEM. The Fourier Transform Infrared (FT-IR) spectrum was obtained by Nicolet 360 spectrometry. Nitrogen adsorption/desorption isotherms studies were prepared using a Micromeritics ASAP 2020 M+C operating at 77 K using the Brunauer-Emmett-Teller (BET) method to determine the surface area.

Detection method

Grinded activated carbon fiber (ACF): The activated carbon fiber (ACF) was finely grounded with ball mill grinder machine to make ACF powder. The achieved ACF powder was smoothed by sieve.

Acid treatment: A moderate amount of ACF powder was added into a mixture of nitric acid:sulfuric acid:distilled water with volume ratio 1:3:1, then stirred with magnetic stirring for 6 h without temperature. The product was washed with distilled water until pH become neutral. The ACF powder with acid treatment was obtained after drying in a vacuum at 100 ºC for 48 h.

Synthesis of $Bi(NO_3)_3{\cdot}5H_2O$-ACF composite: Part A was obtained *via* ultrasonication of a certain amount of $Bi(NO_3)_3{\cdot}5H_2O$ powder in 100 mL distilled water for 30 min (Ultrasonic Processor, VCX 750, 500 Watt, Korea, Power 500 Watt, frequency 20KHz, Amplitude 50%, low intensity). Vigorous stirring of the mixture of parts A and 1 g ACF powder was continued for 6 h at 70 ºC. After a hydrothermal reaction occurred at 100 ºC for 18 h, the product was washed with distilled water until pH become neutral. The $Bi(NO_3)_3{\cdot}5H_2O$-ACF composite was obtained after drying in a vacuum at 100°C for 48 h. Similar samples were prepared corresponds to 0.01, 0.02, and 0.03 mol of $Bi(NO_3)_3{\cdot}5H_2O$ and labeled as ACF-A, ACF-B and ACF-C, respectively.

The typical photocatalytic test carried out at room temperature, the survey samples used in this study was found to be 0.05 g, dissolved in 100 mL rhodamine B solution (200 ppm). Prior to irradiation, the above mixture solution was maintained in a dark box for 2 h to establish the adsorption/desorption equilibrium of organic dyes. The solution was then irradiated with visible light radiation ($\lambda \geq 420$ nm). The first sample was withdrawn at the end of dark adsorption period before switching on the light to determine the rhodamine B concentration in the solution after dark adsorption. The starting point (t = 0) of the reaction was defined as the point where concentration of rhodamine B solution was recorded as c_o. Afterward, these samples were extracted from the solution mixtures in the reactor at regular intervals of 30, 60, 90, 120, and 180 min. The powder was dispersed using a centrifuge machine (10,000 ppm/15 min) before the analysis. The dye concentration in the solution was measured as a function of the irradiation time. The photodegradation of methylene blue and reactive black B solution proceeded following a similar process.

A UV-spectrophotometer (Opizen POP, Korea) was used to analyze the photodegradation of the dye solutions in terms of the concentration (c). A spectrophotometric analysis was performed on each sample of the dye solutions at regular time intervals to obtain the absorbance spectrum. The spectral range was investigated at $\lambda_{max} = 554$, 665 and 591 nm, respectively, for rhodamine B, methylene blue and reactive black B by using a calibration curve since no reaction occurred with the absorption of products at these wavelengths (Table-1). The degradation capacity (η %) was calculated as:

$$\eta\,(\%) = \frac{1-c}{c_o} \times 100$$

The photodegradation of organic dyes was also observed for rhodamine B, methylene blue and reactive black B with (a) ACF-A, (b) ACF-B, and (c) ACF-C, following the same procedure as mentioned above.

TABLE-1
MOLECULAR STRUCTURE AND ABSORBANCE MAXIMUM (λ_{max}) OF THE ORGANIC DYES

Organic dye	Molecular structure	λ_{max} (nm)
Rhodamine B (RhB)	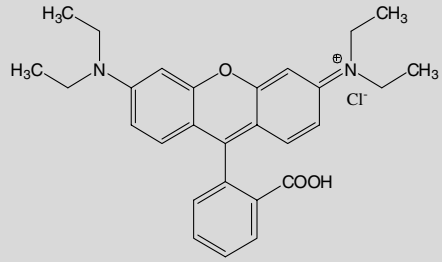	554
Methylene blue trihydrate (MB)	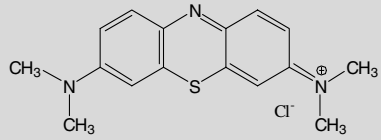	665
Reactive black B (RBB)	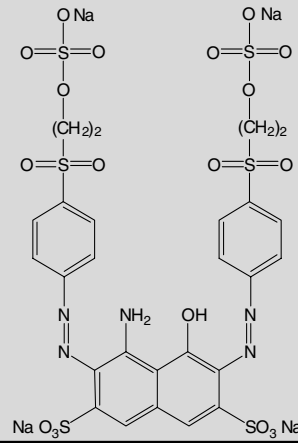	591

RESULTS AND DISCUSSION

The XRD patterns (Fig. 1) of all the samples shows three main diffraction peaks (120), (200) and (121) with the JCPDS file #41-1449, which confirms the presence of monoclinic

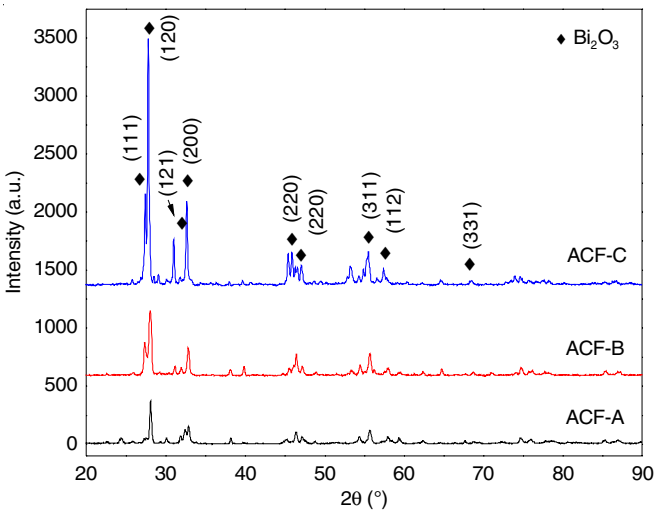

Fig. 1. XRD patterns of the ACF-A, ACF-B and ACF-C composites

Bi_2O_3 [6,27]. All the diffraction peaks are clear and the purity of the nanocomposites was confirmed as no other unexpected peaks found. As there was an increased mole ratio of $Bi(NO_3)_3{\cdot}5H_2O$, the diffraction peaks of Bi_2O_3 was higher and more clearly. The obtained results showed that the prepared composites were almost perfect, with single phase, high crystallinity and purity.

Fig. 2 shows the SEM results of loaded activated carbon fiber (ACF) and the different mole ratios of $Bi(NO_3)_3{\cdot}5H_2O$. According to Fig. 2(a-f), Bi_2O_3 particles with the variety of shapes were successfully covered on the ACF surface. Fig. 2(a-b) exhibited the shape state of 0.01 mol of Bi_2O_3 with 1 g ACF (ACF-A). As the result, Bi_2O_3 particles were presented as the block with disunion morphology. The average diameters of the particle sizes [Fig. 2(a-b)] were found to be around 150 and 220 µm. On the other hand, as the increased mol ratio of $Bi(NO_3)_3{\cdot}5H_2O$, the morphology of the samples was changed from spherical shape [Figs. 2(c-d)], ACF-B) to a disk-like shape with dispersant structure [Figs. 2(e-f), ACF-C]. Their particle sizes were approximately 250-600 and 110-220 µm for ACF-B, ACF-C samples, respectively. The pre-treatment of ACF with acid plays an important role in the morphology of the as-synthesized composites. Besides, the uniformly immobilized with the difference shape of Bi_2O_3 particle on the surface of ACF substrate is promising to bring the variety of photodegradation results of the prepared samples.

The EDX microanalyses of ACF and Bi_2O_3-ACF composites were also recorded as an example in order to obtain the information of the main elements in the prepared composites. According to Figs. 3(a-b), the ACF-C exhibited three kinds of peaks C, O, Bi, and no other impurity was detected. This result means that a combination of ACF and Bi_2O_3 had successfully formed. In Fig. 3a, the strong peak of Bi appeared at 2.6 eV and for oxygen at 0.56 eV as an evidence of the presence of both elements in Bi_2O_3 composite. Table-2 presents the mean amount of elements, which also suggested that the sample had three kinds major elements *viz.*, C, O, and Bi. In ACF case, the EDX was good with 88.28 %, and 11.72 % corresponding to the C and O elements, without the presence of unexpected elements. Besides the presence of C, O, and Bi elements in ACF-A and ACF-B composites with major percent, the small amount impurity elements was detected (Table-2). Beyond the expectation, ACF-C composite was absolutely pure which was rich in Bi (52.39 %) but there is a disparity when compared to C and O elements (22.39 and 25.22 %, respectively). The BET analysis has proceeded and the results are presented in Table-2. The BET surface area of ACF, ACF-A, ACF-B, ACF-C composites was 1125, 950, 920 and 892 m^2/g, respectively. According to above results, it can seen that the surface area was reduced as a result of adding Bi_2O_3 particles in the ACF structure. With an increase in $Bi(NO_3)_2$ mole ratio, the more Bi_2O_3 particles anchored in the ACF, which expected to have a high photocatalytic activity.

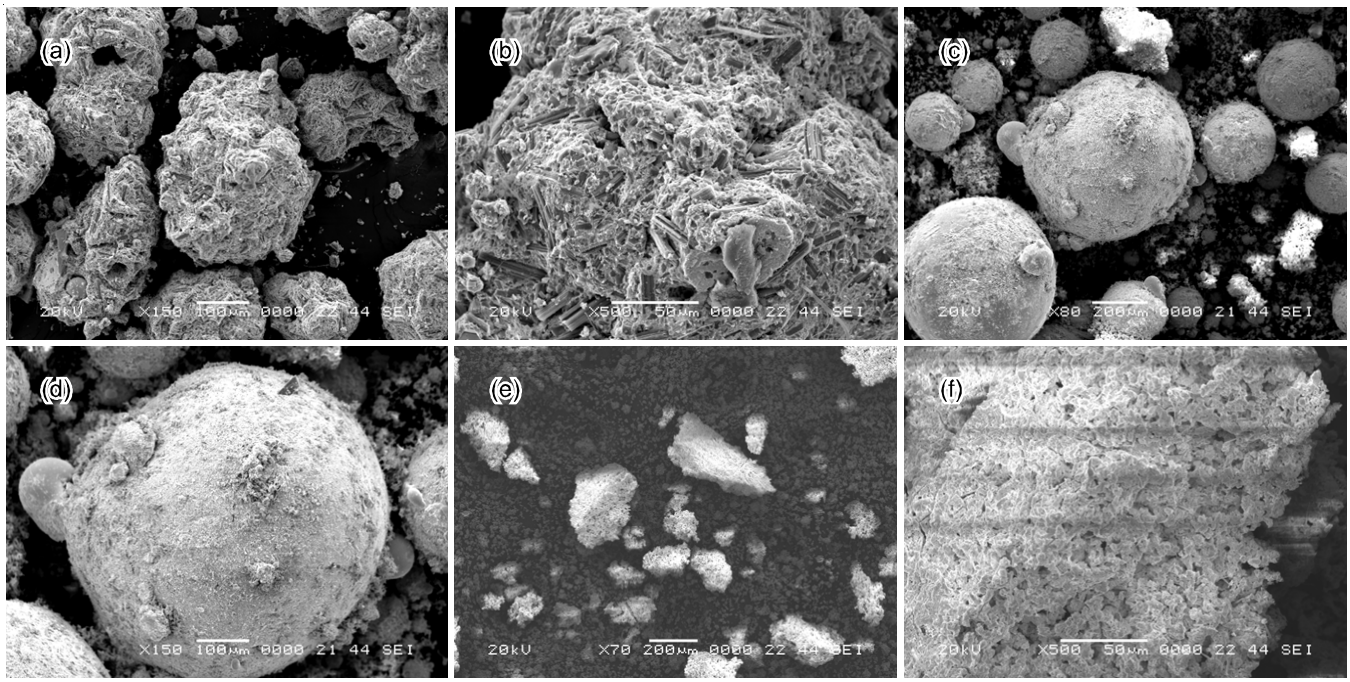

Fig. 2. SEM morphology of ACF-A (a and b), ACF-B (c and d) and ACF-C (e and f) composites

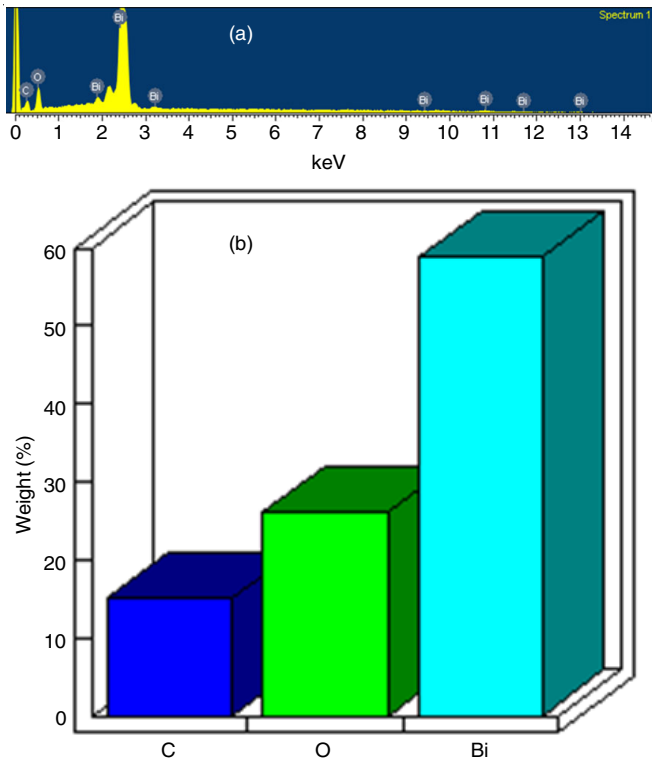

Fig. 3. EDX elemental microanalysis (a) and graphical representation of the quantitative analysis (b) of ACF-C composite

TABLE-2
ELEMENTAL MICROANALYSIS (wt %) OF ACF AND Bi_2O_3-ACF COMPOSITES

Sample	C	O	Bi	Others	S_{BET} (m^2/g)
ACF	88.28	11.72	–	–	1125
ACF-A	59.01	20.24	13.48	7.27	950
ACF-B	23.15	29.32	45.29	2.24	920
ACF-C	22.39	25.22	52.39	–	892

According to the previous report, the FT-IR spectrum of actived carbon fiber shows a variety of peaks that can be attributed to oxygen-containing groups. The peaks centered at 3439, 1630 cm^{-1} assisted the -OH group stretching vibration bands, flexural vibration bands of -OH group, respectively. On the other hand, the peaks located at 2920 and 1122 cm^{-1} corresponded to the stretching vibration bands of the $-CH_2$ group and in-plane flexural vibrations of the -CH group, respectively [28]. For comparison, FT-IR spectrum of Bi_2O_3-activated carbon fiber was surveyed. As the results in Fig. 4, the newly observed characteristic features at 590, 1040 cm^{-1} were obtained as evidence proved that Bi_2O_3 particles covered the actived carbon fiber with the physical interaction, after the hydrothermal reaction. The disappearance of oxygen-containing groups of activated carbon fiber as well as the presence of new peaks corresponding to chemical bonds between Bi_2O_3 and activated carbon fiber [29,30]. The FT-IR spectrum and other results proved that the as-synthesized Bi_2O_3-activated carbon fiber was successfully synthesized.

Photodegradation: The organic dye degradation progressed in two stages. First, the adsorption/desorption equilibrium of organic dyes was established in a dark box for 2 h. Then, the photocatalytic degradation experiment of the dye solutions was conducted under visible light irradiation with different irradiation times (from 0 to 180 min).

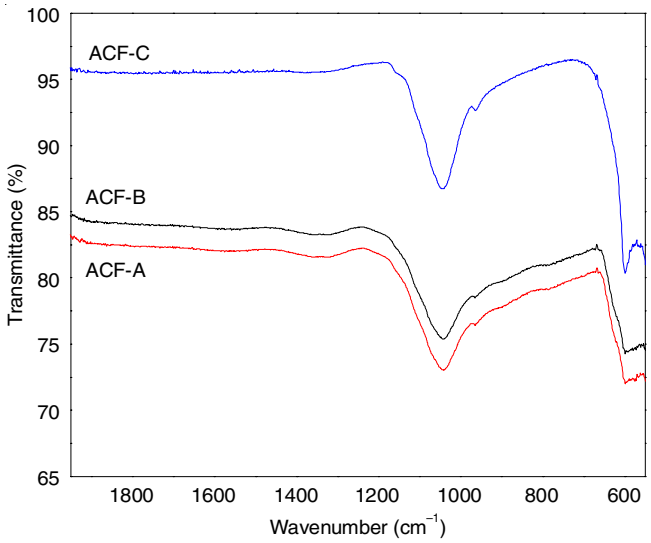

Fig. 4. FT-IR spectra of ACF-A, ACF-B and ACF-C composites

Degradation of rhodamine B: The degradation results of prepared samples with rhodamine B are shown in Fig. 5. Following the adsorption effect in a dark box for 2 h, ACF-A achieved the highest rhodamine B removal with 11.26 %, while ACF-B and ACF-C were removed by around 5.43, and 8.45 %, respectively. For the photocatalytic degradation with 3 h under visible light irradiation, ACF-A still remained the best result with 25.47 % rhodamine B removal, which is better than ACF-B (15.09 %) and ACF-C (13.76 %). The above results showed that ACF-A is the best candidate for the rhodamine B removal than other dyes.

Degradation of methylene blue: The adsorption effect of ACF-A and ACF-B overtook the ACF-C with 11.78, 17.42, and 3.23 % methylene blue removal, respectively (Fig. 6). Hence, ACF-B still kept the best percent of methylene blue removal with 25.44 % after 180 min under visible light irradiation for the For the photocatalytic effect. Beisdes, ACF-A and ACF-C achieved the lower effect with 18.51 and 14.05 %, respectively.

Degradation of reactive black B: The photocatalytic degradation of reactive black B in aqueous solution using prepared composites is shown in Fig. 7. With 9.51 % reactive black B removal, ACF-C shows the best adsorption effect than ACF-A and ACF-B (2.82 %, and 0.75 %, respectively (Fig. 7). Under the visible light, the absorption capacity of ACF-C continued to increase with the increase of irradiation time. The ACF-C composite showed the photodegradation results around 14.47 % removal of reactive black B. Meanwhile, ACF-A and ACF-B composites showed photodegradation results around of 9.47 and 3.55 %, respectively, under the same experimental conditions.

Photocatalytic reactions with different photocatalysts were presented by the Langmuir-Hinshelwood model [31]. The photocatalytic degradation of dye containing different photocatalysts obeys the pseudo-first-order kinetics with respect to concentration of dye solution.

$$-dc/dt = k_{app}c \quad (I)$$

Integration of eqn I (with the restriction of $c = c_o$ at $t = 0$, where c_o is the initial concentration in bulk solution after dark adsorption and t is the reaction time) will lead to the following expected relation:

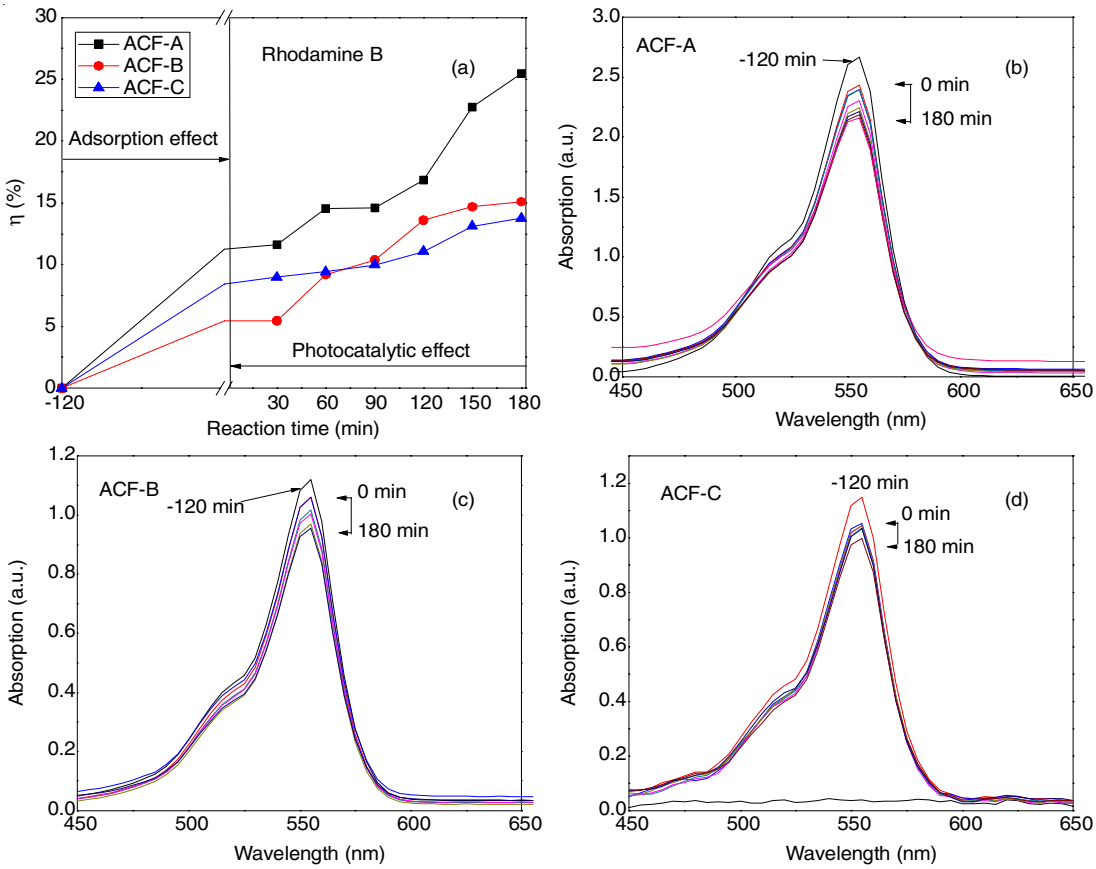

Fig. 5. Degradation of different composites with rhodamine B (RhB) under visible light irradiation. The amount of composites was 0.05 g. The experiments were carried out at 100 mL of 5.0×10^{-5} mol/L mol/L dye concentration with neutral pH

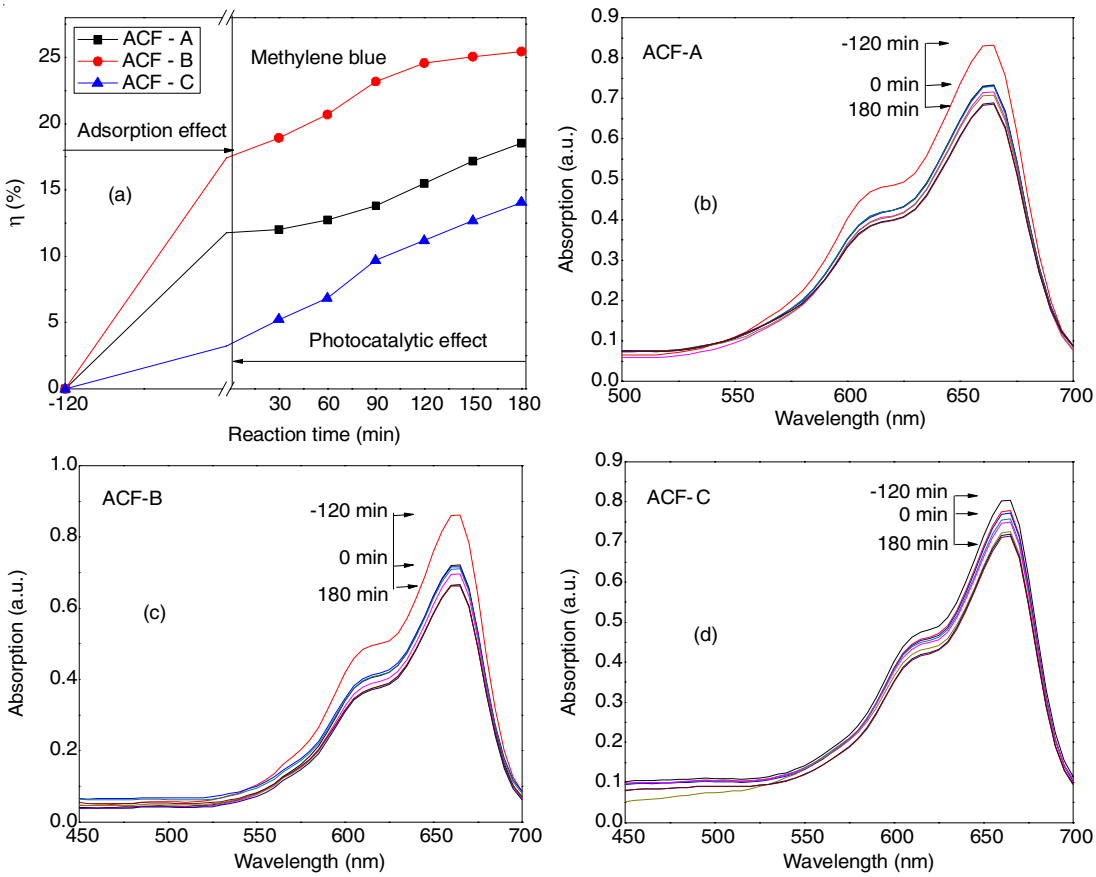

Fig. 6. Degradation of different composites with methylene blue trihydrate under visible light irradiation. The amount of composites was 0.05 g. The experiments were carried out at 100 mL of 5.0×10^{-5} mol/L mol/L dye concentration with neutral pH

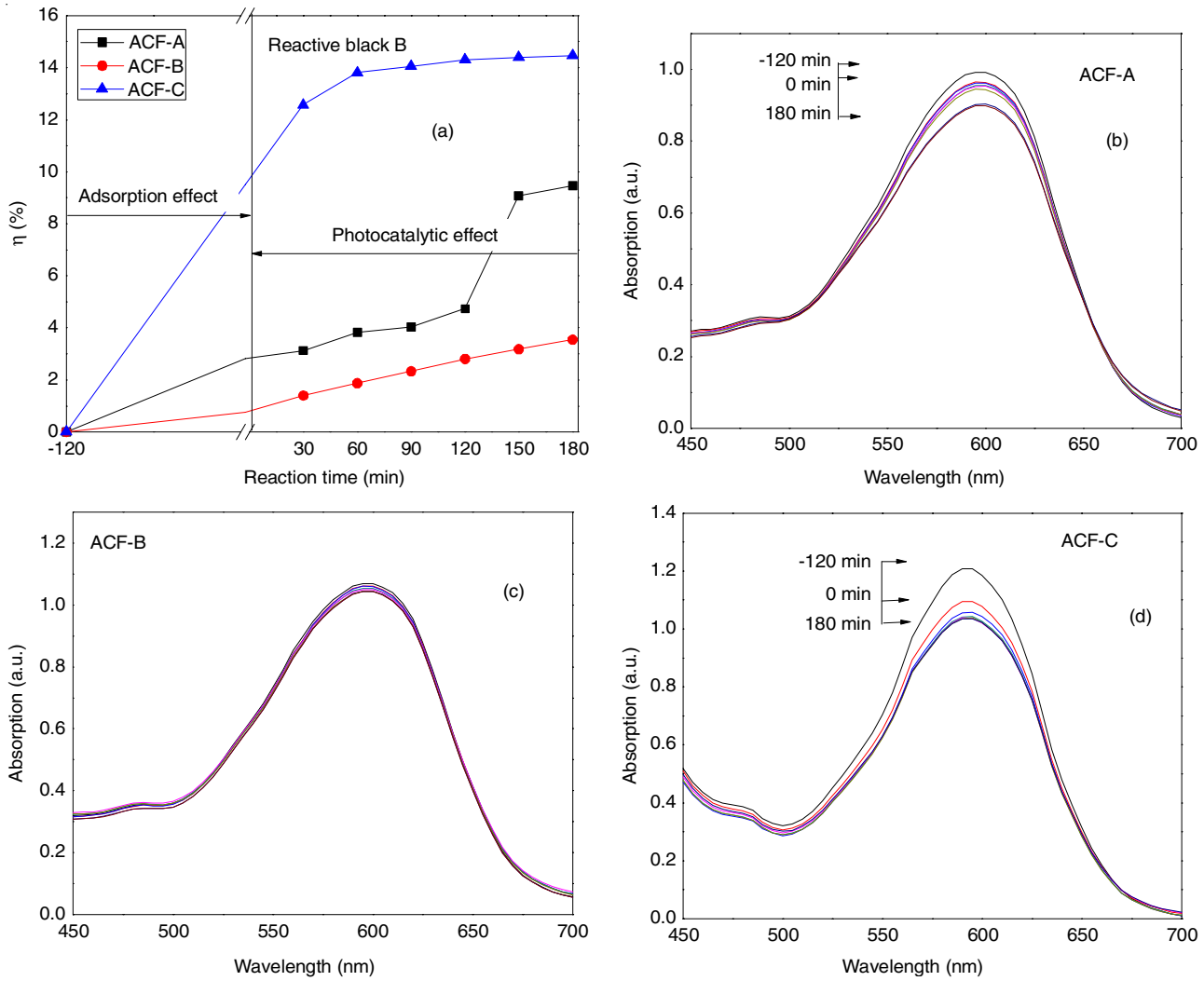

Fig. 7. Degradation of different composites with reactive black B under visible light irradiation. The amount of composites was 0.05 g. The experiments were carried out at 100 mL of 5.0×10^{-5} mol/L mol/L dye concentration with neutral pH

$$-\ln(c/c_o) = k_{app}t \quad \text{(II)}$$

where c and c_o are the reactant concentration at times t = t and t = 0, respectively, and k_{app} and t are the apparent reaction rate constant and time, respectively. According to eqn. II, a plot of $-\ln(c/c_o)$ *versus* t will yield a slope of k_{app}. The results are shown in Fig. 8. The reactive black B degradation rate constant for ACF-B reached 8.0×10^{-3} min^{-1}, and the result was greater than both ACF-A and ACF-C composites. On the other hand, rhodamine B degradation rate constant for ACF-B obtained 6.5×10^{-3} min^{-1}, which higher than other composites. In the methylene blue case, the highest methylene blue degradation rate constant reached 7.9×10^{-3} min^{-1} for ACF-C composite.

It is known that the photocatalytic activity of prepared composite reflects two factors that influence the degradation rate: (a) the adsorption capacity and (b) the decomposition effect through catalysis. In the adsorption case, the great pores and have large surface area of ACF allows a greater amount of guest species over the catalysts, and the reaction will not be limited to photocatalytic surface [32]. Then, the highly enhancement of adsorption as well as the absorption rate of dyes will be occured. Under the visible light irradiation, ACF acts as the free electrons source and Bi_2O_3 particles play a role like a

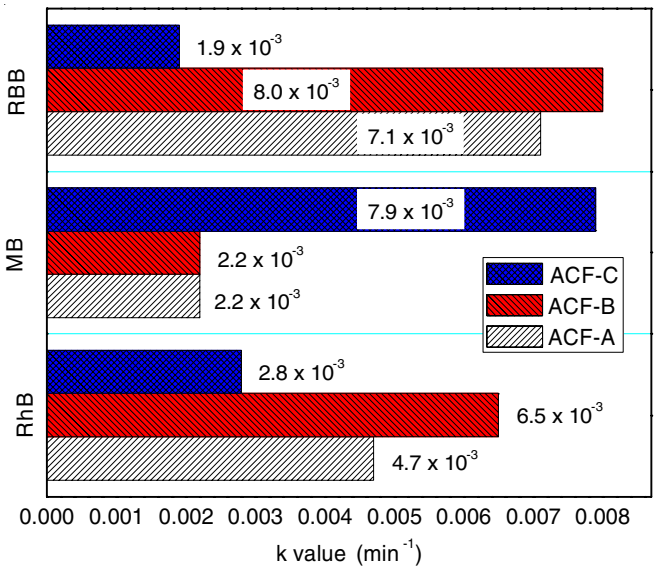

Fig. 8. Kinetic plots for the photodegradation of rhodamine B (RhB), methylene blue trihydrate (MB) and reactive black B (RBB) solution under visible light irradiation over different composites. The amount of composites was 0.05 g. The photodegradation of the rhodamine B, methylene blue trihydrate and reactive black B solution was carried out at 100 mL of 5×10^{-5} mol/L dye concentration with neutral pH

bridge for the transfer of the free electrons from ACF. Besides, ACF can be accept the electrons produced by light irradiation. In the conduction band (CB) and valence band (VB) case, Bi_2O_3 can be also excited to produce electrons and holes under visible light irradiation. The photogenerated electrons of Bi_2O_3 can switch to ACF surface to join the reduction reaction (e^-_{CB}). On the other hand, the photogenerated holes of Bi_2O_3 can also switch the graphene surface to participate in oxidation reactions (h^+_{VB}). With this mechanism, the reduced electron-hole recombination leads to an increase in the catalytic ability. The photogenerated electron-hole shifts to the surface and interacts with substances, such as the hydroxyl group and oxygen, where the adsorption creates free radicals on the surface of the semiconductor. After that, the dye molecules can react with oxygen peroxide radicals $O_2^{\bullet-}$ and hydroxyl radicals $OH^\bullet$ to CO_2, H_2O and mineralization products (Fig. 9) [33-36]:

$$Bi_2O_3\text{-ACF} + h\nu \longrightarrow (Bi_2O_3\text{-ACF})(h^+) + (Bi_2O_3\text{-ACF})(e^-)$$

$$(Bi_2O_3\text{-ACF})(e^-) \longrightarrow Bi_2O_3 + ACF\ (e^-)$$

$$ACF\ (e^-) + O_2 \longrightarrow ACF + O_2^{\bullet-}$$

$$(Bi_2O_3\text{-ACF})(h^+) + OH^- \longrightarrow Bi_2O_3\text{-ACF} + OH^\bullet$$

$$(Bi_2O_3\text{-ACF})(h^+) + H_2O \longrightarrow Bi_2O_3\text{-ACF} + OH^\bullet + H^+$$

$$O_2^{\bullet-} \text{ or } OH^\bullet + \text{organic dyes} \rightarrow CO_2 + H_2O + \text{mineralized products}$$

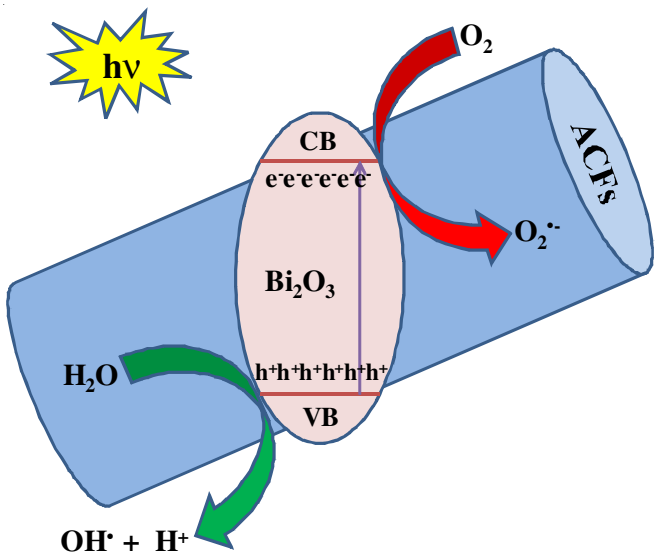

Fig. 9. Scheme of excitation and charge transfer process between Bi_2O_3 particles and ACFs

From the above results, it can seen that ACF exhibited the important role in the decolouration of organic dyes [18]. The anchorage and interaction between Bi_2O_3 particles on the ACF surface is the key role for improved the photodegradation of dyes [37].

Conclusion

A combination of activated carbon fiber (ACF) and Bi_2O_3 particles were successfully synthesized by facile method. The XRD patterns presented the monoclinic phase of Bi_2O_3 particles. Moreover, the morphological characteristics of Bi_2O_3 particles on ACF surface were analyzed through SEM. The EDX quantitative elemental mapping indicates the presence of primary elements such as C, O, and Bi while the FT-IR spectrum shows the structural differences between Bi_2O_3-activated carbon fiber and activated carbon fiber through the removal of oxygen-containing groups and the appearance of a new characteristic band. The photodegradation of rhodamine B, methylene blue and reactive black B dyes using of prepared materials was tested under visible light irradiation. The anchorage and interaction between Bi_2O_3 particles on the ACF surface is the key role for improved photodegradation of dyes.

REFERENCES

1. S.-M. Jin, M.-T. Tang and W.-J. Yang, *J. Central South Univ. Technol.: Nat. Sci.*, **32**, 247 (2001).
2. H.-P. Yang, Y.-N. Fan, M. Lin, B.-L. Xu and Y. Chen, *Chin. J. Catal.*, **23**, 1006 (2002).
3. Z. Jiang, L. Zhang, L. Cai and C. Xia, *Electrochim. Acta*, **54**, 3059 (2009); https://doi.org/10.1016/j.electacta.2008.11.067.
4. S. Sarat, N. Sammes and A. Smirnova, *J. Power Sources*, **160**, 892 (2006); https://doi.org/10.1016/j.jpowsour.2006.02.007.
5. A.A. Tomchenko, *Sens. Actuators B Chem.*, **68**, 48 (2000); https://doi.org/10.1016/S0925-4005(00)00460-3.
6. H. Oudghiri-Hassani, S. Rakass, F.T. Al Wadaani, K.J. Al-Ghamdi, A. Omer, M. Messali and M. Abboudi, *J. Taibah Univ. Sci.*, **9**, 508 (2015); https://doi.org/10.1016/j.jtusci.2015.01.009.
7. J. Cao, X. Li, H. Lin, S. Chen and X. Fu, *J. Hazard. Mater.*, **239-340**, 316 (2012); https://doi.org/10.1016/j.jhazmat.2012.08.078.
8. C. Pan, X. Li, F. Wang and L. Wang, *Ceram. Int.*, **34**, 439 (2008); https://doi.org/10.1016/j.ceramint.2006.10.009.
9. W. Xiaohong, Q. Wei and H. Weidong, *J. Mol. Catal. Chem.*, **261**, 167 (2007); https://doi.org/10.1016/j.molcata.2006.08.016.
10. L. Madler and S.E. Pratsinis, *J. Am. Ceram. Soc.*, **85**, 1713 (2002); https://doi.org/10.1111/j.1151-2916.2002.tb00340.x.
11. H.-O. Jungk and C. Feldmann, *J. Mater. Sci.*, **36**, 297 (2001); https://doi.org/10.1023/A:1004895605613.
12. W.-M. He, Q. Zhen, Q.-Y. Pan and J.-Q. Liu, *J. Funct. Mater.*, **34**, 702 (2003).
13. L. Wei, *J. Central South Univ.: Sci. Technol.*, **36**, 175 (2005).
14. B. Zheng, Z.-G. Ren, J.-Y. Tong and J.-S. Gu, *Chem. Res. Appl.*, **16**, 411 (2004).
15. B. Zheng, A.-H. Pang and J.-S. Gu, *Chem. J. Chin. Univ.*, **26**, 628 (2005).
16. W.L. Hong, F.Q. Zhao, J.-H. Liu and D.-Y. Tian, *Chinese J. Explosives Propellants*, **24**, 7 (2001).
17. M. Mallahi, A. Shokuhfar, M.R. Vaezi, A. Esmaeilirad and V. Mazinani, *Am. J. Eng. Res.*, **3**, 162 (2014).
18. P.F. Fu, Y. Luan and X.G. Dai, *J. Mol. Catal. Chem.*, **221**, 81 (2004); https://doi.org/10.1016/j.molcata.2004.06.018.
19. A. Fujishima and K. Honda, *Nature*, **238**, 37 (1972); https://doi.org/10.1038/238037a0.
20. A. Fujishima, T.N. Rao and D.A. Tryk, *J. Photochem. Photobiol. Photochem. Rev.*, **1**, 1 (2000); https://doi.org/10.1016/S1389-5567(00)00002-2.
21. H.K. Son, S. Sivakumar, M.J. Rood and B.J. Kim, *J. Hazard. Mater.*, **301**, 27 (2016); https://doi.org/10.1016/j.jhazmat.2015.08.040.
22. G.B. Baur, I. Yuranov and L. Kiwi-Minsker, *Catal. Today*, **249**, 252 (2015); https://doi.org/10.1016/j.cattod.2014.11.021.
23. Z. Shen, W. Wang, J. Jia, J. Ye, X. Feng and A. Peng, *J. Hazard. Mater.*, **84**, 107 (2001); https://doi.org/10.1016/S0304-3894(01)00201-1.
24. J. Li, Z. Yu, M. Gao and X. Cai, *Water Air Soil Pollut.*, **97**, 367 (1997); https://doi.org/10.1023/A:1026426516790.
25. S. Yao, J. Li and Z. Shi, *Particuology*, **8**, 272 (2010); https://doi.org/10.1016/j.partic.2010.03.013.
26. M. Li, B. Lu, Q.-F. Ke, Y.-J. Guo and Y.-P. Guo, *J. Hazard. Mater.*, **333**, 88 (2017); https://doi.org/10.1016/j.jhazmat.2017.03.019.
27. J. Xia, M. Tang, C. Chen, S. Jin and Y. Chen, *Trans. Nonferrous Met. Soc. China*, **22**, 2289 (2012); https://doi.org/10.1016/S1003-6326(11)61462-3.

28. Z. Jiang, B. Huang, Z. Lou, Z. Wang, X. Meng, Y. Liu, X. Qin, X. Zhang and Y. Dai, *Dalton Trans.*, **43**, 8170 (2014); https://doi.org/10.1039/c4dt00483c.
29. Y.N. Wang, K.J. Deng and L.Z. Zhang, *J. Phys. Chem. C*, **115**, 14300 (2011); https://doi.org/10.1021/jp2042069.
30. D.C.T. Nguyen, K.Y. Cho and W.-C. Oh, *RSC Advances*, **7**, 29284 (2017); https://doi.org/10.1039/C7RA03526H.
31. Y. Li, X. Li, J. Li and J. Yin, *Water Res.*, **40**, 1119 (2006); https://doi.org/10.1016/j.watres.2005.12.042.
32. Y. Yao, L. Wang, L. Sun, S. Zhu, Z. Huang, Y. Mao, W. Lu and W. Chen, *Chem. Eng. Sci.*, **101**, 424 (2013); https://doi.org/10.1016/j.ces.2013.06.009.
33. R. Raghav, P. Aggarwal and S. Srivastava, *AIP Conf. Proc.*, **1724**, 020078 (2016); https://doi.org/10.1063/1.4945198.
34. J.P. Espinós, J. Morales, A. Barranco, A. Caballero, J.P. Holgado and A.R. González-Elipe, *Catalysts. J. Phys. Chem. B*, **106**, 6921 (2002); https://doi.org/10.1021/jp014618m.
35. W.-C. Oh, M. Chen, K. Cho, C. Kim, Z. Meng and L. Zhu, *Chin. J. Catal.*, **32**, 1577 (2011); https://doi.org/10.1016/S1872-2067(10)60264-1.
36. D.C.T. Nguyen, K.-Y. Cho and W.-C. Oh, *Appl. Surf. Sci.*, **412**, 252 (2017); https://doi.org/10.1016/j.apsusc.2017.03.248.
37. C.H. Ao and S.C. Lee, *Appl. Catal. B*, **44**, 191 (2003); https://doi.org/10.1016/S0926-3373(03)00054-7.